Analysis of Inelastic Proton Scattering from ^{14}N Between 8.60 and 26.0 MeV*

L. F. Hansen, S. M. Grimes, J. L. Kammerdiener,* and V. A. Madsen‡
Lawrence Livermore Laboratory, Livermore, California 94550
(Received 16 July 1973)

The elastic and inelastic proton differential cross sections for ^{14}N have been measured at 8.6, 10.6, 12.6, and 14.6 MeV. The variation with energy of the cross sections, as well as the shape of the angular distributions, indicated that the contribution of compound processes to some of the inelastic cross sections was not negligible at these energies. Fits to the elastic scattering data yielded proton optical parameters, which were used in calculating transmission coefficients for a Hauser-Feshbach calculation of the compound nuclear contribution to the inelastic cross sections. These data corrected for compound effects, and measurements for scattering to the 2.31- and 3.95-MeV levels at 18.0, 21.0, 23.0, and 26.0 MeV reported in the literature, were analyzed with a microscopic coupled-channel calculation. The purpose of the analysis was to find out how sensitive the calculations were to the wave functions used for ^{14}N, to the values of the effective two-body force, and to the channels coupled. The results were also compared to a simple distorted-wave Born-approximation (DWBA) calculation. Calculations for the 3.95- and 7.03-MeV level were also carried out assuming a weak-coupling model for ^{14}N, two $p_{1/2}$ nucleons coupled to a ^{12}C core. This collective model gave over-all better agreement with the measured differential cross sections for these levels than the DWBA or the microscopic coupled-channel calculation.

[NUCLEAR REACTIONS ^{14}N(p,p), ^{14}N(p,p'), $E=8.6$, 10.6, 12.6, and 14.6 MeV; measured $\sigma(E,\theta)$; $\theta=15$–$165°$; coupled-channel analysis. ^{14}N(p,p'), $E=18$, 21, 23, 26 MeV, previous data compared with coupled-channel calculation.]

INTRODUCTION

Several authors[1-10] have compared measured and calculated differential cross sections for proton inelastic scattering from ^{14}N at intermediate energies, $8<E_p<30$ MeV. The calculations[5-7] carried out with an effective two-body force have shown rather conclusively the need for a tensor force. In addition, it has been found that a coupled-channel calculation gives better agreement with the measurements than a distorted-wave Born-approximation (DWBA) calculation. Unfortunately, calculations have had only marginal success[7,9,10] in reproducing the shapes of the measured angular distributions. Agreement is especially poor for the recent measurements at 14.5 MeV carried out by Curtis *et al.*[9]

In the present work, proton elastic and inelastic differential cross sections have been measured at 8.6, 10.6, 12.6, and 14.6 MeV. The variation with energy of the cross sections, as well as the shape of the angular distributions, indicated that the contribution of compound processes to some of the inelastic cross sections was not negligible at these energies. The presence of compound contributions in the cross sections could account for the disagreement found[9] at 14.6 MeV between the measurements and calculations. Consequently, a meaningful comparison with the calculations was possible only when the compound contribution was subtracted from the measurements. In the work reported in this paper, these compound inelastic cross sections were calculated with the Hauser-Feshbach equation. The calculation of the direct inelastic cross sections was carried out with a microscopic and a macroscopic model for the nuclear interaction, using in both cases the Oregon State University coupled-channel code.[11] The microscopic coupled-channel calculation was studied (1) as a function of the wave functions for ^{14}N reported in the literature,[12-14] (2) as a function of the potentials used in the effective two-body force,[15,16] and (3) as a function of the coupling scheme between the inelastic levels involved in the calculation. In the macroscopic calculation a collective model was used in the calculation of the 3.95- and 7.03-MeV levels. The ground state and first two excited levels of ^{14}N, 2.31 and 3.95 MeV, together with the 7.03-MeV level were described in a weak-coupling model, as two $p_{1/2}$ nucleons coupled to the ^{12}C core. Since only spin-independent $l=0$ and $l=2$ transitions are included in the collective model, the transition to the 2.31-MeV level, which requires a spin flip, was calculated only with the microscopic model.

As will be shown, the wave functions for ^{14}N which include only p-shell configurations, such as Visscher-Ferrell[12] and Cohen-Kurath[13] wave

functions, are unable to reproduce the shape of the inelastic proton cross section from the 3.95-MeV level, although they agree with the differential cross sections for the 2.31- and 7.03-MeV levels reasonably well. The Freed-Ostrander[14] wave functions, in which *s-d* shell configurations are also included, account only at forward angles for the measured differential cross sections for the 2.31-MeV level, while the shapes of the angular distributions for the inelastic scattering from the 3.95-MeV level are improved over those calculated with only *p*-shell wave functions.[12,13] Finally, the differential cross sections to the 7.03-MeV level calculated with Freed-Ostrander[14] wave functions are very close in shape to those given by Cohen-Kurath[13]; however, the magnitude is lower by a factor of about 5. No attempt was made to fit the other inelastic levels since at the energies of these measurements, with the exception of the 4.91-MeV level, all show appreciable contributions from compound processes. Since it is expected that at higher energies compound contributions would become negligible, the measurements of Lutz, Heikkinen, and Bartolini[10] for the ground-state, 2.31- and 3.95-MeV levels at 18, 21, 23, and 26 MeV were also analyzed with the micro-

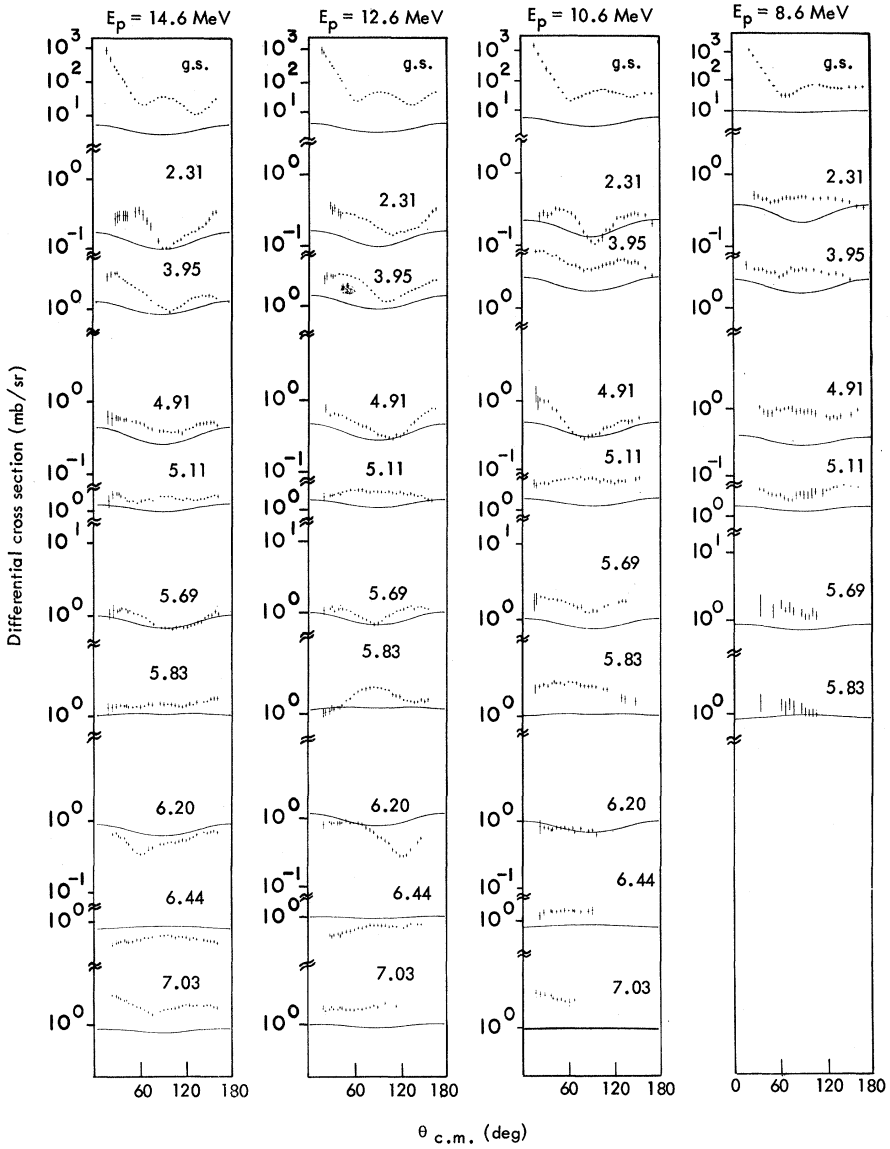

FIG. 1. Differential cross sections for the elastic and inelastic scattering of the protons, measured at 8.6, 10.6, 12.6, and 14.6 MeV. The solid curves are the Hauser-Feshbach calculations of the compound scattering.

scopic coupled-channel calculation and, as expected, the agreement with the measurements improved.

EXPERIMENTAL METHOD

The measurements were carried out with the proton beam from the Livermore 90-in. variable-energy cyclotron. The incident proton energies were 8.55, 10.6, 12.6, and 14.6 MeV at the center of the gas cell. A target of natural N_2 gas was used with a purity of 99.99%. The gas cell, 2.54 cm in diameter, had a continuous 290° window made of 0.000 254-cm-thick Havar (cobalt-based alloy) foil. The cell, located at the center of the scattering chamber, was filled to a pressure of 600-mm Hg at 20°C; temperature and pressure were continuously monitored during the runs. The volume of gas seen by the detectors was defined by a set of vertical slits 0.32 cm wide at 7.62 cm from the center of the gas cell and by square edge collimators of 0.32 cm by 0.4 cm placed at the face of the detectors. These were located 27.94 cm from the center of the gas cell. Outgoing protons were detected and identified with three lithium-drifted silicon ΔE-E counter telescopes utilizing particle-identification circuits described elsewhere.[17] The detectors were cooled to −30°C to minimize leakage currents. The three telescopes were mounted at fixed 10° intervals with respect to one another and served to reduce the data collection time and eliminate possible systematic errors in the cross sections due to detector performance. The differential cross sections were measured from 15–165° in 5° intervals. Proton spectra from the telescopes were stored in the memory of a PDP8 computer which also served as a multichannel analyzer. The analysis of the data was performed with a CDC-6600 computer program which calculated the cross sections to the levels by integrating Gaussian fits to each peak in the proton spectrum. During the runs, the three identifier spectra were displayed continuously to verify that the separation between protons and deuterons did not change during the runs.

EXPERIMENTAL RESULTS

Figure 1 shows the spectra for the elastic and inelastic scattered protons from ^{14}N at 8.6-, 10.6-, 12.6-, and 14.6-MeV incident proton energies. Among the inelastic levels, only the 3.95 and 7.03 MeV show systematic forward peaking and these also have comparatively large cross sections with respect to the other inelastic levels. The 2.31-MeV level shows a direct contribution only at and above 10.6 MeV. The other inelastic levels at the lower energies show appreciable contribution from compound processes, as indicated by the maxima or minima at 90° of many of the angular distributions. Large resonance effects in the excitation functions of the inelastic levels up to 7.03-MeV excitation energy in ^{14}N have been measured by Messelt[4] between 7 and 11 MeV, which is also consistent with the large compound contributions observed in the differential cross sections measured in the present work.

The integrated inelastic cross sections for the levels shown in Fig. 1 were obtained by Legendre polynomial fits to the angular distributions. In Table I are tabulated the total cross sections for inelastic levels up to 7.03-MeV excitation energy, together with other measurements reported in the literature for energies close to these measure-

TABLE I. Total cross sections for the protons inelastically scattered from ^{14}N as function of incident proton energy.

E_L (MeV) \ U (MeV)	$\sigma(E_L,U)$ (mb) 2.31	3.95	4.91	5.10	5.69	5.83	6.21	6.44	7.03	Ref.
8.52	8.0									1
8.6	10.7	44.6	7.9	23.2	11.7	17.5				a
10.2		77.0	5.6	34.0	16.3	25.0	7.6	12.7	27.2	3
10.5	3.2	57.8								1
	3.7	67.0	5.0	30.0	17.0	20.0	7.0	11.0	24.0	2
10.54	3.4	58.6	5.5	41.6	17.7	40.9	6.2	19.2	29.2	4
10.6	4.2	69.3	5.7	43.1	17.9	40.0	6.7	19.0	28.9	a
12.6	3.9	27.0	5.4	25.7	12.6	28.3	6.6	9.0	25.9	a
14.1	3.4	22.5								1
14.5	2.9	17.5	3.3	14.0	8.8	19.1	5.8	6.0	23.6	9
14.6	3.2	18.5	4.8	19.0	8.7	19.2	4.7	5.9	27.9	a

[a] Present work.

ments. At 14.6 MeV the angular distributions for the 7.97-, 8.06-, 8.49-, 8.91-, and 9.17-MeV levels were also obtained, but these measurements were carried only to 90.0° (with the exception of the 7.97-MeV level that was measured to 125° and the 9.17-MeV level to 60°). The integrated cross sections for these levels are 8.1, 1.3, 13.2, 9.6, and 8.1 mb, respectively. The errors in the total cross sections for the inelastic levels up to 7.03 MeV given in Table I are 10% or less. For the higher excited levels, the given cross sections are upper limits and the errors can be as large as 30%, since they were obtained by assuming symmetry around 90°.

ANALYSIS OF THE DATA

A. Optical-Model Fits to the Elastic Scattering

The fits to the measured elastic cross sections were done using the optical-model code LOKI,[18] which includes a least-squares search routine.

The optical potential $U(r)$ used in LOKI is given by the standard expression

$$U(r) = V_c - V\frac{1}{e^x+1} - i\left\{\left[\alpha W - 4(1-\alpha)W_D\frac{d}{dx'}\right]\frac{1}{e^{x'}+1}\right\} + \left(\frac{\hbar}{m_\pi c}\right)^2 V_s(\vec{\sigma}\cdot\vec{L})\frac{1}{r}\frac{d}{dr}\frac{1}{e^x+1}, \quad (1)$$

where

$$x = (r - r_0 A^{1/3})/a,$$

$$\chi' = (r' - r_0' A^{1/3})/a',$$

$$0 \leq \alpha \leq 1.$$

The Coulomb potential V_c corresponds to the potential from a uniformly charged sphere of radius $1.25A^{1/3}$ fm. Optical parameters of Perey[19] and Becchetti and Greenlees[20] for protons were taken as starting values. Since in both cases the parameters have been obtained for much heavier nuclei, the procedure used was to fix the geometrical parameters and to search for the optimum values of the potentials V, W_D, and V_s by minimizing χ^2:

$$\chi^2 = \sum_{i-1}^{n}\{[\sigma_{th}(\theta_i) - \sigma_{exp}(\theta_i)]/\Delta\sigma_{exp}(\theta_i)\}^2. \quad (2)$$

Finally, to see if the χ^2 value could be reduced further, the requirement of fixed geometrical parameters was dropped, and all parameters were varied to determine the best set. The resulting values are called the LOKI set. Because of the low energies of the protons, compound elastic corrections were carried out. The optical parameters obtained at each stage were used to calculate transmission coefficients for the Hauser-Feshbach calculation of compound elastic scattering; the calculated compound elastic cross section was then subtracted from the measured elastic cross section and this angular distribution was fitted to yield the optical parameters for the next stage. After three successive iterations, the χ^2 values remained nearly constant and the search was ended. In Fig. 1 the magnitude of these corrections for the elastic scattering are shown. Table II gives the optical parameters and the χ^2 obtained for these three different sets. For the high-energy measurements, 18, 21, 23, and 26 MeV,[10] the optical parameters reported by Lutz, Heikkinen, and Bartolini[10] were used.

B. Hauser-Feshbach Calculations

The compound nucleus contribution to the ^{14}N-(p,p') cross sections was calculated with the Hauser-Feshbach[21] equation. This relation is based on the assumption that formation and decay of the compound nucleus are independent processes and is valid only if the lifetime of the compound state

TABLE II. Optical-model parameters obtained after search for the elastic scattering data.

Optical-model set	Energy (MeV)	V (MeV)	W_D (MeV)	V_s (MeV)	r_0 (fm)	a (fm)	r_0' (fm)	a' (fm)	χ^2	σ_{n-e} (mb)
Perey	14.6	49.41	6.28	2.84	1.25	0.65	1.25	0.65	388	595
Becchetti		56.93	5.63	2.31	1.17	0.75	1.32	0.51	408	612
LOKI		53.05	6.38	3.21	1.205	0.605	1.03	0.53	102	535
Perey	12.6	48.99	3.75	4.67	1.25	0.65	1.25	0.65	65.2	465
Becchetti		52.65	3.67	4.03	1.17	0.75	1.32	0.51	163	515
LOKI		51.61	3.59	5.83	1.205	0.605	1.03	0.53	71.9	400
Perey	10.6	48.26	2.73	6.42	1.25	0.65	1.25	0.65	94.6	395
Becchetti		51.46	2.76	6.54	1.17	0.75	1.32	0.51	179	451
LOKI		51.71	2.44	6.48	1.205	0.605	1.03	0.53	53.2	327
Perey	8.6	46.66	1.74	6.19	1.25	0.65	1.25	0.65	8.24	321
Becchetti		48.95	1.90	6.70	1.17	0.75	1.32	0.51	121	386
LOKI		49.84	1.61	5.32	1.205	0.605	1.03	0.53	13.6	296

is long enough for the compound nucleus to reach equilibrium before decay occurs. Aside from possible difficulties with this assumption for a light nucleus, there are other complications in such a calculation in this mass region. Because the decay width to all possible final states must be included in the calculation of the branching ratios, level schemes and optical parameters for the systems reached by α-particle, ^{3}He, deuteron, and neutron as well as proton emission are required. For reactions on targets with $A > 30$, it is generally assumed that the levels can be represented by a level-density formula and that the optical parameters can be approximated by those obtained from studies of the average behavior of optical potentials as a function of A. In the case of the ^{14}N(p, p') reaction, specific level schemes are required for the nuclei ^{11}C, ^{12}C, ^{13}N, ^{14}O, and ^{14}N, since the level densities are too small to be represented analytically. The accuracy of the calculation thus depends crucially on the reliability of the level information for these nuclei. It is not expected that optical parameters for such nuclei are described as well by "average" potentials as would those for heavy nuclei; nonetheless, because ^{11}C, ^{13}N, and ^{14}O are unstable, some extrapolation is required. These difficulties make the calculated compound cross sections more uncertain than would be the case for a heavier nucleus, but the results should be useful in determining whether the angular distributions and relative magnitudes of the cross sections to the various levels are in better agreement with statistical model predictions than with corresponding direct-reaction calculations.

The equation used in calculating angular distributions for statistical processes has been obtained by Douglas and McDonald[22] from the relations derived by Wolfenstein[23] and Hauser and Feshbach.[21]

This expression is

$$\sigma_{ab}(\theta, E_b)\, dE_b\, d\Omega = \frac{1}{K_a^{\,2}} \frac{1}{(2I_1+1)(2i_1+1)} \sum_{L S, S_2 I_2} B_L(bE_b S_2 a S_1)\, P_L(\cos\theta)\, dE_b\, d\Omega\,, \tag{3}$$

where

$$B_L(b, E_b S_2 a S_1) = \sum_J \sum_{l_1} \sum_{l_2} \frac{1}{4} (-1)^{S_2 - S_1} \frac{T^J_{al_1}(E_a) T^J_{bl_2}(E_b) \rho_b(\epsilon_{b'} I_2)}{\sum_{b' l'_2 S'_2 I'_2} \int_0^{\epsilon_{b'\max}} d\epsilon_{b'} T^J_{b' l_2'}(E_{b'}) \rho_{b'}(\epsilon_{b'} I'_2)}\,. \tag{4}$$

In Eq. (3), $\sigma_{ab}(\theta, E_b)$ is the cross section for emission of particle b with energy E_b at an angle θ from a compound nucleus formed by bombarding the target nucleus with particle a, with wave number K_a. I_1 and i_1 are the spins of the target nucleus and projectile a, respectively, while I_2 and i_2 are the corresponding quantities in the outgoing channel. The parameters S_1 and S_2 denote the channel spins in the entrance and exit channels. $T^J_{bl}(E_b)$ is the transmission coefficient in channel b at an energy E_b and $\rho_b(\epsilon_b, I_2)$ is the level density at an excitation energy ϵ_b and for spin I_2 of the residual nucleus reached by emission of particle b. The level schemes listed in Ajzenberg-Selove and Lauritsen[24, 25] were used in place of a functional form for the level densities. Because of the small Coulomb barrier, levels at excitation energies up to 14 MeV in ^{14}N must be included, while for the final nuclei ^{11}C, ^{12}C, ^{14}O, and ^{13}N levels up to 11.0-, 13.7-, 8.0-, and 3.5-MeV excitation energy, respectively, were included. Isospin coupling was also included in the Hauser-Feshbach calculation.[26] In the present case this coupling modifies the widths only to $T = 1$ final states in ^{14}O and ^{14}N, with couplings of $\frac{2}{3}$ to $n + {}^{14}$O and $\frac{1}{3}$ to $p + {}^{14}$N $(T = 1)$. Because some levels have presumably not yet been observed, the values for the calculated cross sections to the levels of interest may be too large, particularly at the highest energies. This effect could account for the large compound cross sections obtained for the 6.20- and 6.44-MeV levels for 12.6- and 14.6-MeV protons as can be seen in Fig. 1.

Transmission coefficients for the proton channel were calculated with the potentials obtained from the optical-model fits to the elastic scattering as described earlier. This procedure yielded values for the optical potentials at 8.6, 10.6, 12.6, and 14.6 MeV. For lower energies the optical parameters were obtained as follows: the geometrical parameters were left fixed and the spin-orbit potential set equal to the value at 8.6 MeV; the real potential was obtained by assuming a linear variation with incident energy with the slope determined over the range 8.6 to 14.6 MeV. If this same procedure had been used for the imaginary potential, a value of zero would have resulted for W_D for all bombarding energies below about 5 MeV. It was therefore assumed that the imaginary potential was constant below 8.6 MeV. This assumption is not necessarily in agreement with the potentials which would be obtained by analyzing elastic scat-

tering at energies lower than 8 MeV. Because the level density in the compound system is low for a light nucleus at excitation energies slightly above the nucleon binding energy, the imaginary potential is expected to be small, while this potential for the same incident energy on an excited nucleus (which is the case in a statistical calculation) could be considerably larger.

The potentials for the α particles were obtained from Schwartz *et al.*[27] They derived the optical parameters for the α+C system from a study of the ^{12}C(^{3}He, α)^{11}C reaction and assumed that strengths of the potentials and geometrical parameters were independent of energy. The ^{3}He optical potentials were those reported by Baugh *et al.*[28] Although these authors measured the elastic scattering from ^{3}He on ^{12}C at 29 MeV, they found values which were very close to those obtained by Bassel[29] in fitting ^{3}He data at 12, 22, and 29 MeV. For the neutrons, the optical parameters are those reported by Bauer *et al.*[30] for the $n+^{14}$N system and cover the energy range from 8 to 14 MeV. In contrast to the proton results, a linear extrapolation of the imaginary potential below 8 MeV does not result in a value of zero for positive energies. This is possibly due to the fact that the excitation energy in the $n+^{14}$N system is about 3.5 MeV higher than the corresponding energy in the $p+^{14}$N system for the same bombarding energy. Compound level-density effects in the low-energy absorption cross section should be smaller for neutrons than for protons. It was therefore decided to use a linear extrapolation for both the real and imaginary potential below 8 MeV; the geometrical parameters and the spin-orbit potential were assumed to be constant. Finally, the deuteron optical potentials were those of Alty *et al.*[31] for 18-MeV deuterons on ^{16}O.

Satchler[32] and Moldauer[33] have shown that the traditional statistical calculation should be modified by the addition of a width-fluctuation correlation coefficient, W_{cc}. This factor is present because the partial widths in both entrance and exit channels are expected to fluctuate. If the fluctuations are correlated, as is the case for the elastic channel in which entrance and exit widths are identical, the expectation value of the product of the two widths will not be equal to the product of the expectation values. The width-fluctuation correlation coefficient indicates the degree of enhancement and is defined as

$$W_{cc'} = \frac{\langle \Gamma_c \Gamma_{c'} \rangle}{\langle \Gamma_c \rangle \langle \Gamma_{c'} \rangle} . \quad (5)$$

Satchler[32] and Moldauer[33] have shown that W_{cc} should be equal to three at low energies and equal to two at high energies for the usual width distributions, while if $c \neq c'$, $W_{cc} = 1$. In the present calculations W_{cc} was taken equal to two, in which case the effect of this correlation is to multiply all nonelastic cross sections by $1/(1+\sigma_{cc}/\sigma_{\text{react}})$ and the elastic cross sections by $2/(1+\sigma_{cc}/\sigma_{\text{react}})$, where σ_{react} is the reaction cross section and σ_{cc} the elastic cross section.

The compound calculations for the elastic and inelastic proton scattering from ^{14}N are shown by the solid lines in Fig. 1. The accuracy of these calculations is estimated to be of the order of 30 to 40%. They were calculated with the proton optical parameters given by the LOKI set in Table II, since these values gave over all a lower value of χ^2 at all energies. These parameters gave the lowest values for the calculated compound cross sections, while Perey's parameters gave the highest values. Another source of uncertainty in the calculated cross sections is the choice of optical parameters for the other exit channels. For example, if the potential for deuterons of Schiffer *et al.*[34] had been used in the calculations, the compound width for deuteron emission would have been lower by 30 to 40%, which would raise the compound contribution to proton cross sections by about 10%.

C. Coupled-Channel Calculations

The inelastic scattering cross sections, using both microscopic and macroscopic models, were calculated using the Oregon State University coupled-channel code.[11] Inelastic scattering calcula-

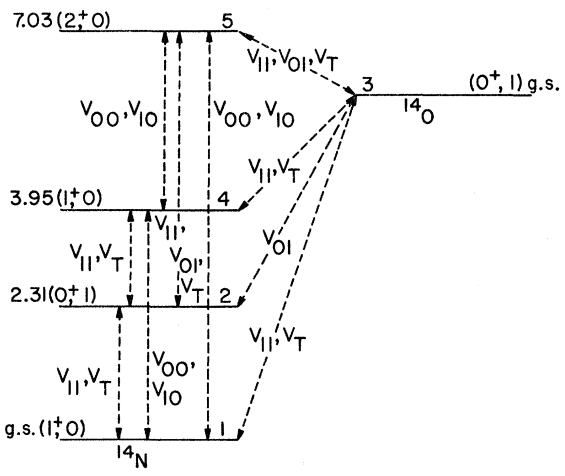

FIG. 2. Levels in ^{14}N and ^{14}O included in the microscopic coupled-channel calculation. The dashed lines show the couplings among the levels. The components of the effective two-body force, V_{00}, V_{10}, V_{01}, and V_T, that contribute to the transitions between the levels, are also shown.

tions with DWBA [9,10] have been unable to reproduce the angular distributions of the protons from the $p+{}^{14}$N system. The aim in the analysis of the present data was to find out if introducing coupling between the various inelastic and charge-exchange channels can improve the calculations.

Microscopic Model

In coupled-channel calculations the interaction is treated to all orders in contrast to the perturbation-theory approach of DWBA, which includes only the first-order term. Higher-order terms are included automatically by coupling intermediate states through which the reaction is likely to proceed. In the present work coupling between the ground-state (gs), 2.31-, 3.95-, and 7.03-MeV levels in ^{14}N and the gs (2.31 analog) in ^{14}O were included. Figure 2 shows the couplings among these levels. The effects of the different couplings will be discussed later.

The coupling matrices were calculated using the microscopic formalism of Madsen.[35] The total wave function, ψ, is expanded in terms of a product basis consisting of the nuclear wave functions times the projectile wave functions

$$\psi=\frac{1}{r}\sum_{\substack{JMn\\ j_n l_n}} R_{Jnl_n j_n}(r)(Y_{l_n j_n}\phi_{I_n})_{JM}, \tag{6}$$

where

$$[Y_{l_n j_n}\phi_{I_n}]_{JM}=\sum_{m_j} C(j_n I_n J; m_j M_n M) Y_{l_n j_n m_n}\phi_{I_n M_n} \tag{7}$$

and

$$Y_{l_n j_n m_j}=[i^{l_n} Y_{l_n}(\hat{r})\,\Sigma_s]_{j_n m_j}. \tag{8}$$

In Eqs. (6), (7), and (8) $R_{Jnl_n j_n}(r)$ is a radial coefficient depending on the distance r between center of masses of target and projectile; ϕ_{I_n} is the nuclear wave function for channel n with spin I_n; J is the total angular momentum of the system and m, its z projection.

Putting Eq. (6) into the Schrödinger equation for the total wave function ψ, $H\psi=E\psi$, one gets:

$$\left[-\frac{\hbar^2}{2m}\left(\frac{d^2}{dr^2}+\frac{l_n(l_n+1)}{r^2}\right)+V_{nn}(r)-E+E_n\right]R_{Jnl_n j_n}$$
$$=-\sum_{\substack{n'\neq n\\ l_{n'} j_{n'}}} V_{nn'}(r)R_{Jn'l_{n'} j_{n'}}, \tag{9}$$

where

$$V_{n'n}=\langle[Y_{l_{n'} j_{n'}}\Phi_{I_{n'}}]_{JM}|\,V\,|[Y_{l_n j_n}\Phi_{I_n}]_{JM}\rangle. \tag{10}$$

E is the incident energy of the projectile and E_n is the excitation energy or Q value of the level n. In the calculation the diagonal terms of the potential, V_{nn}, are taken to be optical-model potentials given by Eq. (1) and are calculated using the optical parameters given in Table II. The off-diagonal terms $V_{n'n}$ are obtained from a microscopic two-body potential given by

$$V(r)=[(V_{00}+V_{10}\vec{\sigma}_1\cdot\vec{\sigma}_2)+(V_{01}+V_{11}\vec{\sigma}_1\cdot\vec{\sigma}_2)\vec{\tau}_1\cdot\vec{\tau}_2]v_c(r)$$
$$+V_T S_{12}\vec{\tau}_1\cdot\vec{\tau}_2 v_T(r), \tag{11}$$

where

$$v_c(r)=e^{-\alpha_c r}/\alpha_c r, \tag{12}$$

$$V_T(r)=E(\alpha_T r)-(\beta/\alpha_T)^3 E(\beta r), \tag{13}$$

$$E(xr)=\left[1+\frac{3}{xr}+\frac{3}{(xr)^2}\right]\frac{e^{-xr}}{xr}\quad \text{for } x=\alpha,\beta, \tag{14}$$

and

$$S_{12}=\left[\frac{3(\vec{\sigma}_1\cdot\vec{r})(\vec{\sigma}_2\cdot\vec{r})}{r^2}-\vec{\sigma}_1\cdot\vec{\sigma}_2\right]. \tag{15}$$

The strengths $V_{ST}=(V_{00}, V_{10}, V_{01}, V_{11})$ correspond to changes S or T of the z component of the spin and isospin, respectively. These potential strengths are also written in the literature as V_0, V_σ, V_τ, and $V_{\sigma\tau}$, respectively. There are selection rules[35] that determine which components of the microscopic two-body force enter in the scattering between given levels. In Fig. 2 these are shown for the present study. Two different effective forces were used in the calculations to investigate the sensitivity of cross sections and angular distributions to the assumed force. One of these was derived from the Kallio-Kolltveit interaction[15] (KK interaction) by Petrovich *et al.*,[36] using a 1-F range, α_c for the central force. The second force was obtained from Cohen and Kurath[16] (CK) effective matrix elements, normalized to a central force range $\alpha_c=0.71$ using the relation given by Schmittroth[5] to transform from a V_{TE}, V_{SE}, V_{TO}, V_{SO} to a V_{00}, V_{10}, V_{01}, V_{11} representation. In Table III the strengths of the potentials for the KK and CK interactions are given. It was found that for a given wave function and coupling scheme, the main difference in the use of these two effective forces was in the magnitude of the cross sections. Figure 3 shows calculations carried out with Cohen-Kurath[13] wave functions, coupling each level only to the ground state. The cross sections for the 2.31-MeV level were very close in magnitude, while those for the 3.95- and 7.03-MeV level calculated with the CK effective force[16] were normalized by 4.9 and 1.63, respectively. For the 3.95-MeV level the transition is predominantly an electric quadrupole type ($L=2$, no spin flip) so the cross sections are roughly in the ratio of the

TABLE III. Strengths of the potentials for the KK and CK interactions.

Interaction	V_{00} (MeV)	V_{10} (MeV)	V_{01} (MeV)	V_{11} (MeV)	V_T (MeV)	α_c (fm^{-1})	α_T (fm^{-1})	β_T (fm^{-1})
Kallio-Kolltveit	−36.2	6.23	17.8	12.1	4.0	1.0	0.714	4.0
Cohen-Kurath	−7.22	6.04	8.04	7.13	4.0	0.714	0.714	4.0

square of the strength of the V_{00} term, taking into account the difference in range. For the 7.03-MeV level the transition includes both electric quadrupole and magnetic dipole type ($L=0$, spin flip). Since the CK interaction has a larger V_{10} strength the weakness of the quadrupole transition is partly compensated for, and the cross sections are more nearly equal.

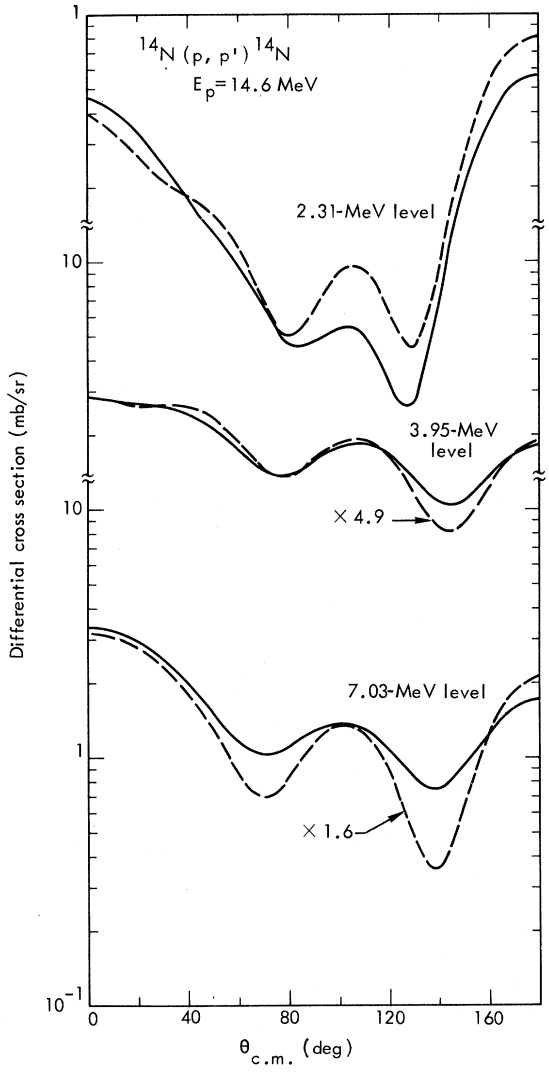

FIG. 3. Differential cross sections for the inelastic protons at 14.6 MeV calculated with Cohen-Kurath wave functions, coupling each level only to the ground state. The solid curves were obtained using the Kallio-Koltveit interaction and the dashed curves with the Cohen-Kurath interaction.

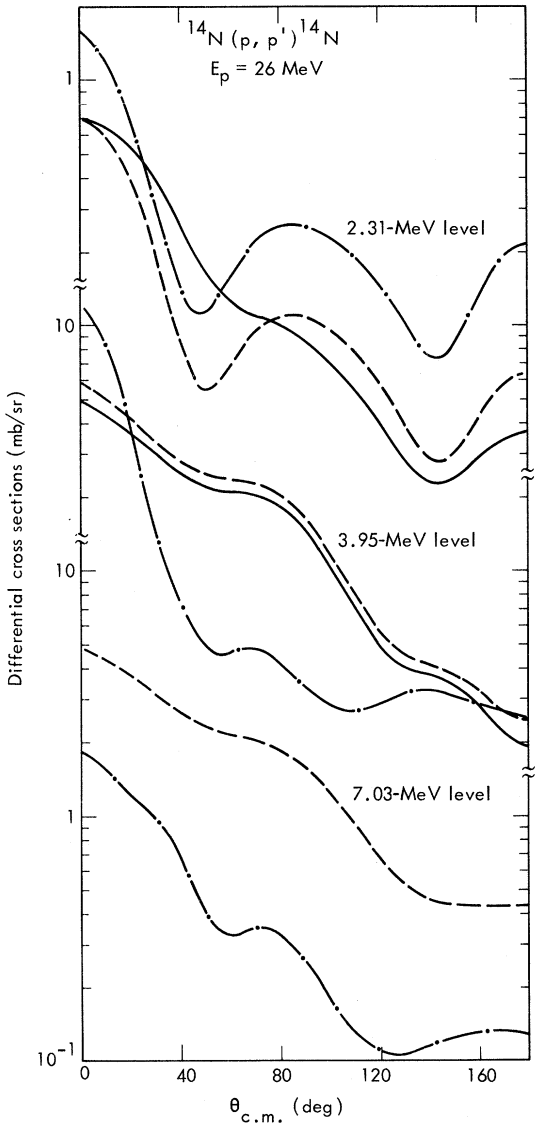

FIG. 4. Comparison of the differential cross sections for the inelastic protons scattered from the 2.31-, 3.95-, and 7.03-MeV levels obtained with a DWBA calculation using Visscher-Ferrell (——), Cohen-Kurath (----), and Freed-Ostrander (—·—·—) wave functions.

The spectroscopic amplitudes used in the microscopic calculations were obtained for three different sets of wave functions for ^{14}N, to test the sensitivity of the calculations to the shell configurations. These wave functions were those of Visscher and Ferrell[12] (VF) for the three first states of ^{14}N and the ground state of ^{14}O, those of Cohen and Kurath[13] (CK) for the above states plus the 7.03-MeV level, and those of Freed and Ostrander[14] (FO) for all the states. The two first wave functions[12,13] are pure p-shell wave functions, while

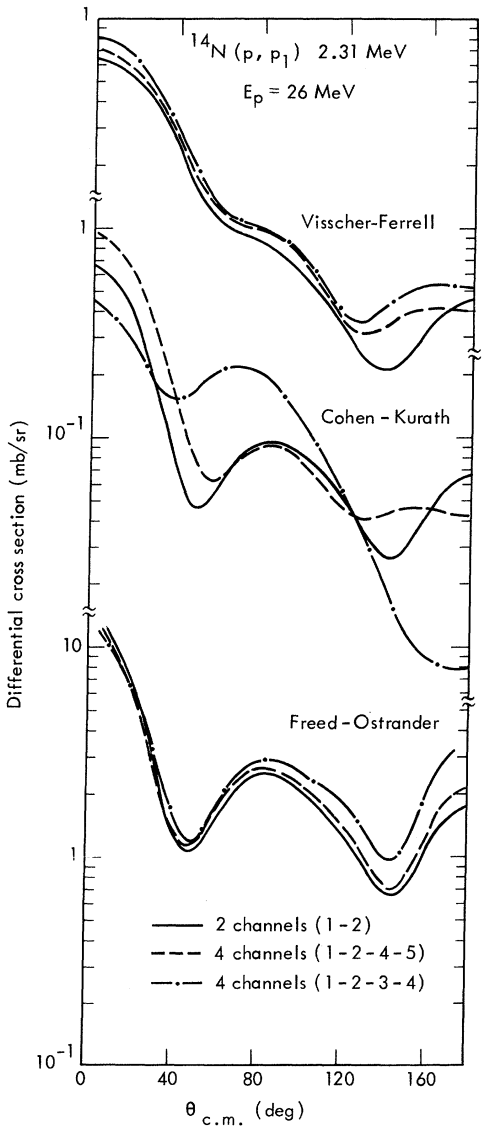

FIG. 5. Comparison of the differential cross sections for the inelastic protons scattered from the 2.31-MeV level as function of the levels included in the microscopic coupled-channel calculation (see Fig. 2), with Visscher-Ferrell, Cohen-Kurath, and Freed-Ostrander wave functions.

Freed and Ostrander include also s-d shell configurations but exclude $p_{3/2}$ holes. *A priori*, it is expected that only the two sets of the p-shell wave functions will be able to reproduce properly the scattering to the 2.31-MeV level, since it is well known[37] that the explanation of the β transition from the analogous ground state of ^{14}C to the ground state of ^{14}N requires configurations with holes in the $p_{3/2}$ shell even if $2s$, $1d$ configurations are included. The anomalously long lifetime for this β decay ($\log ft = 9.03$) has been adequately accounted for by VF and CK wave functions. Figure 4 shows the differential cross sections for the 2.31-, 3.95-, and 7.03-MeV levels, obtained with the above wave functions for a DWBA calculation. (The microscopic coupled-channel calculation reduces to a DWBA calculation if all the strengths of the potentials in the effective two-body force are made close to zero. This condition is satisfied if all the interaction strengths are divided by 10^3.) As expected, the VF and CK wave functions give similar results for the 2.31- and 3.95-MeV levels. The inclusion of the s-d shell configuration in FO wave functions changes the shape of the angular distributions for the first two excited levels, while for the 7.03-MeV level the difference between CK and FO wave functions is primarily in the magnitude of the calculated cross sections.

The sensitivity of the calculations to the couplings between the levels was also studied. In Fig. 2, the ground state and 2.31-MeV levels of ^{14}N are labeled states 1 and 2; state 3 is the ground state of ^{14}O and states 4 and 5 are the 3.95- and 7.03-MeV levels, respectively, in ^{14}N. This nomenclature is also used in Figs. 5, 6, and 7 in describing the coupling. The ^{14}O ground state was included in the coupling for consistency, since isospin considerations[38] show that the coupling to this charge-exchange channel is stronger by $\sqrt{2}$ than the inelastic transition to the 2.31-MeV state. In Fig. 5 are shown the changes in the angular distributions obtained for the scattering from the 2.31-MeV level as function of the coupling among the levels for the VF, CK, and FO wave functions. This state is the most sensitive to the coupling used in the calculations, particularly for CK wave functions, where the shapes of the angular distributions are quite distinctive for some of the couplings. This is not the case for the 3.95-MeV level seen in Fig. 6, where the shape of the angular distributions remained almost independent of the coupling. The same is more or less true for the 7.03-MeV level shown in Fig. 7. Here all the coupling combinations predict almost identical angular distributions, with exception of the simplest coupling, 7.03-gs, where a small difference can be observed for CK wave functions. The above features are present

at all the incident proton energies reported in this work.

The main difference between the coupled-channel calculations and the DWBA calculations shown in Fig. 4 is in the magnitude of the cross sections. The coupling increases the cross section as much as 20% for the 2.31-MeV level, and produces reductions of about the same amount for the 3.95- and 7.03-MeV levels. Changes less than 10% in the magnitude of the cross sections occur for different couplings. In Table IV and V are given the calculated cross sections as function of the coupling, and the measured cross sections of Lutz, Heikkinen, and Bartolini.[10] For the differential cross sections measured in the present work, the comparison becomes less meaningful since the corrections for compound contributions are an appreciable fraction of the measurements. Minor changes in shape and displacement of the minima by as much as 10° can also be observed between the DWBA and the coupled-channel calculations. For the elastic scattering the main differences in the shape of the angular distributions calculated with DWBA or a coupled-channel procedure occur at the minima as can be seen in Fig. 8. The DWBA angular distributions calculated, for the optical parameters given by the LOKI set in Table II, with the coupled-channel code,[11] give identical results to the values obtained with the LOKI code.[18] However, when the elastic scattering cross sections

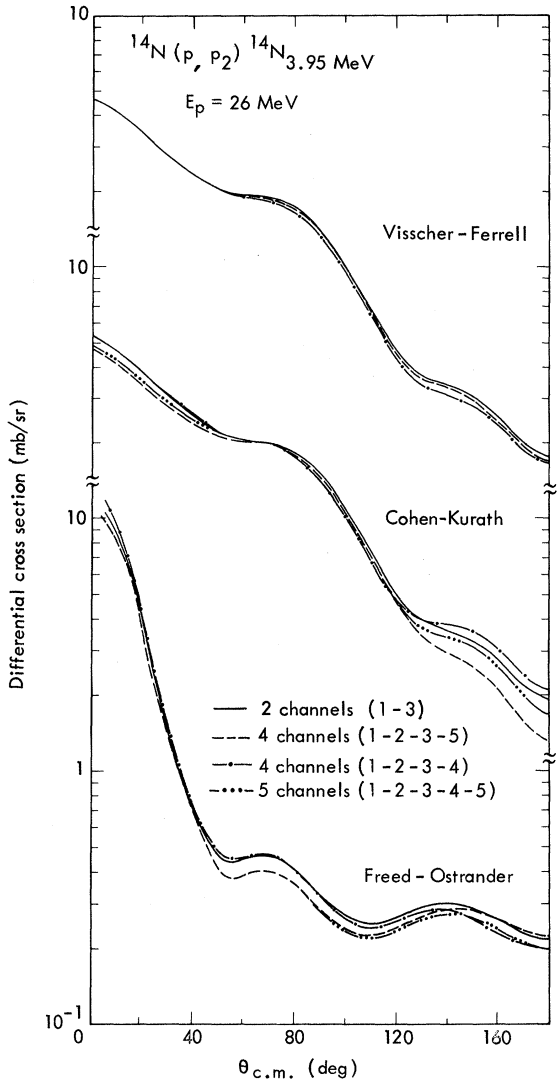

FIG. 6. Comparison of the differential cross sections for the inelastic protons scattered from the 3.95-MeV level as function of the levels included in the microscopic coupled-channel calculation (see Fig. 2), with Visscher-Ferrell, Cohen-Kurath, and Freed-Ostrander wave functions.

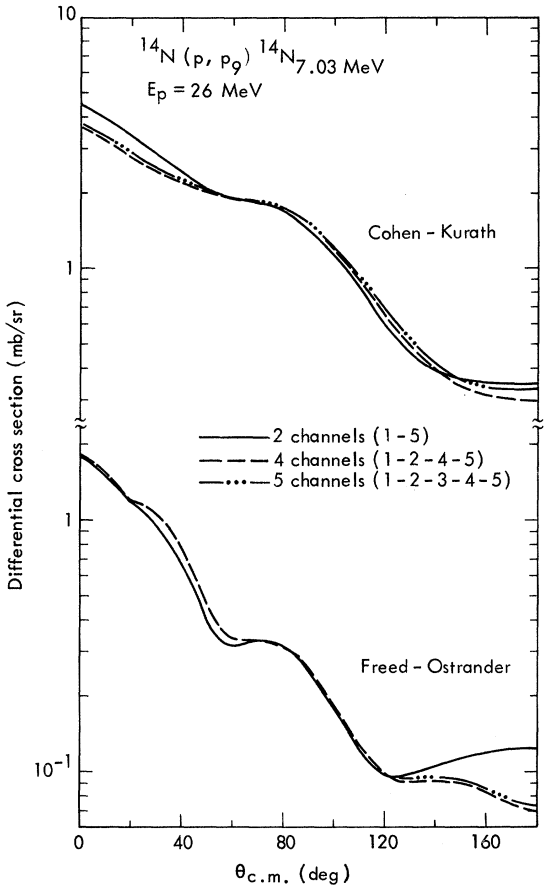

FIG. 7. Comparison of the differential cross sections for the inelastic protons scattered from the 7.03-MeV level as function of the levels included in the microscopic coupled-channel calculation (see Fig. 2), with Visscher-Ferrell, Cohen-Kurath, and Freed-Ostrander wave functions.

TABLE IV. Calculated cross sections for the 2.31-MeV level as function of the wave function for ^{14}N and the levels included in the coupled-channel calculations.

E_p (MeV)	σ_{exp}[a]	Wave function[b]	DWBA σ (mb)	Channels coupled in the calculation σ_{1-2}	$\sigma_{1-2-3-4}$	$\sigma_{1-2-4-5}$	$\sigma_{1-2-3-4-5}$
18.0	1.9	VF	2.19	1.89	2.59	2.35	...
		CK	1.62	1.48	2.27	2.12	2.04
		FO	3.50	3.24	4.16	3.39	4.25
21.0	1.3	VF	1.92	1.64	2.06	1.89	...
		CK	1.46	1.33	1.92	1.70	1.78
		FO	3.13	2.87	3.47	2.99	3.55
23.0	1.3	VF	1.89	1.62	2.01	1.84	...
		CK	1.46	1.33	1.92	1.67	1.79
		FO	3.19	2.93	3.49	3.04	3.56
26.0	0.7	VF	1.62	1.40	1.70	1.56	...
		CK	1.26	1.11	1.68	1.41	1.58
		FO	2.75	2.54	2.96	2.64	3.04

[a] Reference 10.

[b] VF, Visscher-Ferrell wave functions (Ref. 12); CK, Cohen-Kurath wave functions (Ref. 13); FO, Freed-Ostrander wave functions (Ref. 14).

are calculated in a coupled-channel mode, the imaginary potentials listed in Table III had to be reduced by 20 to 30%, between 14.6 and 8.6 MeV, to be able to obtain the same reaction cross sections shown in the table. This reduction in the strength of W_D is due to the fact that the coupled-channel calculation includes certain inelastic channels explicitly, while in the fits to the elastic scattering alone, the imaginary potential accounts for all the inelastic processes.

Since the coupled-channel calculations do not include exchange effects, and since the importance of exchange has been firmly established for DWBA calculations, it was assumed[39] that it must be also included in a coupled-channel calculation. The primary effect of exchange is to put into the direct calculation an L-dependent factor. In coupled-channel calculations the same enhancement factors are appropriate.[39] Since the V_{00} (spin–isospin-independent) part of the effective two-body force (Eq. 11) is involved primarily in $L=2$ transitions, and the V_{10} (V_σ) and V_{11} ($V_{\sigma\tau}$) primarily in $L=0$ transitions, these strengths have been corrected by appropriate exchange factors. These corrections are equivalent to multiplying[40] the V_{00} strength by 1.85 and the V_{10}, V_{01}, and V_{11} by 1.43. These factors have been taken from Fig. 1 of Ref. 40.

Furthermore, Rose, Häusser, and Warburton[37] have shown that Visscher-Ferrell and Cohen-Kurath wave functions, where only p-shell configura-

TABLE V. Calculated cross sections for the 3.95-MeV level as function of the wave functions for ^{14}N and the levels included in the coupled-channel calculation. In the last column are given the cross sections calculated with a weak-coupling model for ^{14}N.

E_p (MeV)	σ_{exp}[a]	Wave function[b]	DWBA σ (mb)	Channels coupled in the calculation σ_{1-2}	$\sigma_{1-2-3-4}$	$\sigma_{1-2-4-5}$	$\sigma_{1-2-3-4-5}$	Collective mode
18.0	12.9	VF	26.1	23.1	22.3	22.7	...	
		CK	29.6	26.4	24.8	24.6	25.1	11.2
		FO	11.3	10.8	11.0	10.2	10.3	
21.0	10.4	VF	21.9	19.7	19.1	19.4	...	
		CK	24.8	22.3	21.2	20.4	20.8	10.1
		FO	9.83	9.42	9.66	8.54	8.64	
23.0	10.0	VF	22.1	20.0	19.4	19.7	...	
		CK	24.9	22.6	21.5	20.6	21.0	9.62
		FO	9.94	9.54	9.75	8.65	8.73	
26.0	7.0	VF	18.7	17.0	16.7	16.9	...	
		CK	21.1	18.6	18.4	17.7	18.0	7.99
		FO	8.62	8.32	8.42	7.58	7.63	

[a] Reference 10.

[b] VF, Visscher-Ferrell wave functions (Ref. 12); CK, Cohen-Kurath wave functions (Ref. 13); FO, Freed-Ostrander wave functions (Ref. 14).

tions are assumed, (s^4p^{10}) do not reproduce the measured strengths of the $E2$ transitions, and that collective enhancement of the calculated $E2$ rates is needed. From Table IX in Ref. 37, the ratio of the measured-to-calculated electric quadrupole widths is roughly equal to 4 for the transitions from the 3.95-MeV level to the ground state, for 7.03-MeV level to the ground state, and from the 7.03-MeV level to the 3.95-MeV level. To account for these effects in the calculations, with the above wave functions, the V_{00} strength was multiplied by a factor of 2 in addition to the exchange correction. The new values for the strengths for the effective two-body force using Kallio-Kolltveit interaction [15] became $V_{00} = -134.0$ MeV, $V_{10} = 8.90$ MeV, $V_{01} = 25.5$ MeV, and $V_{11} = 17.3$ MeV. It is emphasized that

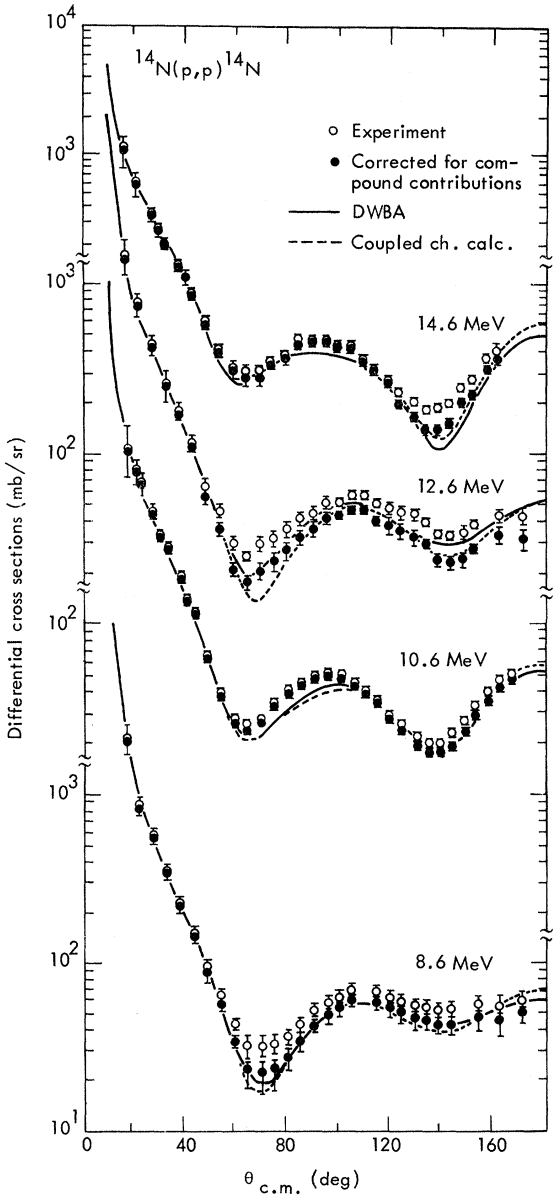

FIG. 8. Differential cross sections for the elastic scattering measured at 8.6, 10.6, 12.6, and 14.6 MeV (Φ). The filled circles are the measurements minus the calculated compound elastic cross sections. The solid curves were obtained with a DWBA calculation and the dashed curves with a coupled-channel calculation.

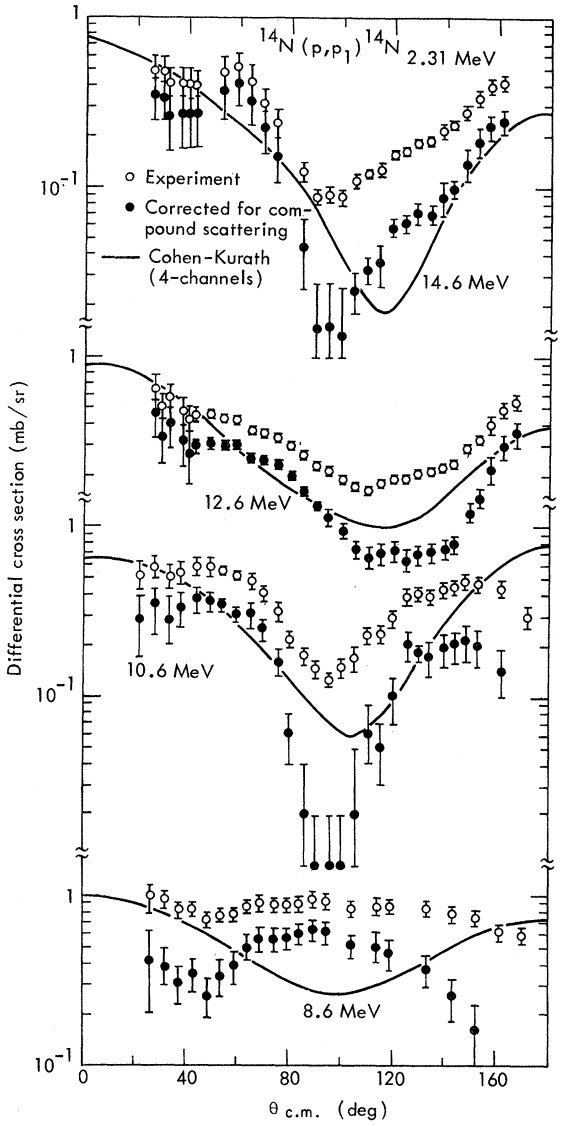

FIG. 9. Differential cross sections for the inelastic protons from the 2.31-MeV level, measured at 8.6, 10.6, 12.6, and 14.6 MeV (Φ). The filled circles are the measurements corrected for the calculated compound inelastic cross section to this level. The solid curves were obtained with a four-channel microscopic coupled calculation (1-2-3-4) with Visscher-Ferrell wave functions (14.6 MeV) and Cohen-Kurath wave functions (12.6, 10.6, and 8.6 MeV).

these are not arbitrary corrections but are required by what is known about exchange effects and about the known deficiency of $1p$ shell-model wave fucntions in accounting for E_2 strengths. Although exchange effects are assumed to also play a role in the tensor force, the value used is an empirical one obtained by fitting direct DWBA results to experiment. Thus exchange effects are implicitly included. From a comparison of the magnitudes of the multipole moments obtained with Cohen-Kurath wave functions for the gs→3.95 and gs→7.03 transitions and those obtained with Freed-Ostrander wave functions, it was found that V_{00} had to be multiplied by 2.5 for the latter wave functions to correct the deficiency in the E_2 strength, instead of the value of 2 used for Cohen-Kurath wave functions.

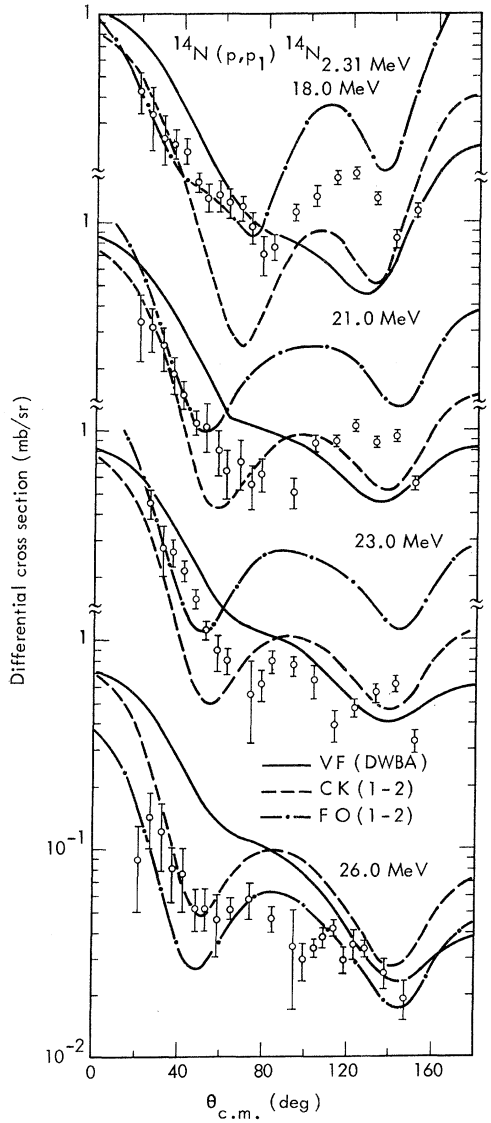

FIG. 10. Differential cross sections for the inelastic protons from the 2.31-MeV level, measured (Ref. 10) at 18.0, 21.0, 23.0, and 26.0 MeV (Φ). The solid curve is a DWBA calculation with Visscher-Ferrell wave function; the dashed curve is a two-channel microscopic coupled calculation (1-2) with Cohen-Kurath wave functions; and (—·—) with Freed-Ostrander wave functions.

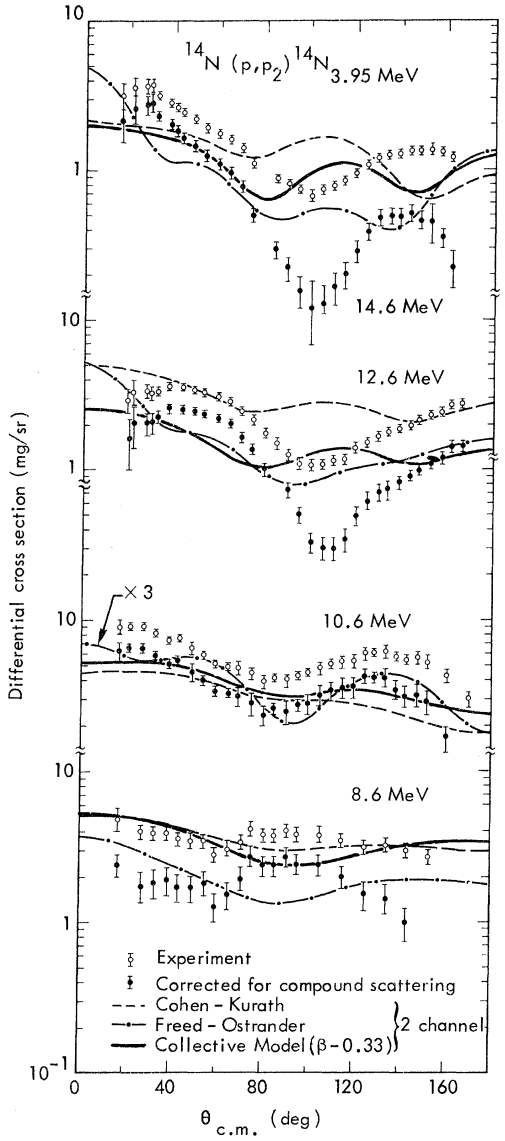

FIG. 11. Differential cross sections for the inelastic protons from the 3.95-MeV level, measured at 8.6, 10.6, 12.6, and 14.6 MeV (Φ). The filled circles are the measurements corrected for the calculated compound inelastic cross section to this level. The curves are a two-channel (1-4) microscopic calculation with Cohen-Kurath wave function (---) and with Freed-Ostrander wave function (—·—). The solid curve is a two-channel macroscopic calculation with $\beta = 0.33$.

In Figs. 9 to 13 a comparison between the microscopic coupled-channel calculations carried out for the 2.31-, 3.95-, and 7.03-MeV levels and the measurements are shown. All these calculations used the Kallio-Kolltveit interaction corrected for exchange effects and electric quadrupole enhancement. For the 2.31-MeV levels at 8.6-, 10.6-, 12.6-, and 14.6-MeV incident proton energies, the calculations correspond to those with a 1-2-3-4 coupling scheme (gs ^{14}N-2.31 MeV-gs ^{14}O-3.95 MeV). Although the calculations gave very similar results for Visscher-Ferrell and Cohen-Kurath wave functions, the theoretical curves plotted in Fig. 9 correspond to a subjective best choice among the fits with these two wave functions. The 14.6 and 8.6 MeV angular distributions are those calculated with VF wave functions; the 12.6 and 10.6 MeV with Cohen-Kurath. It can be seen that

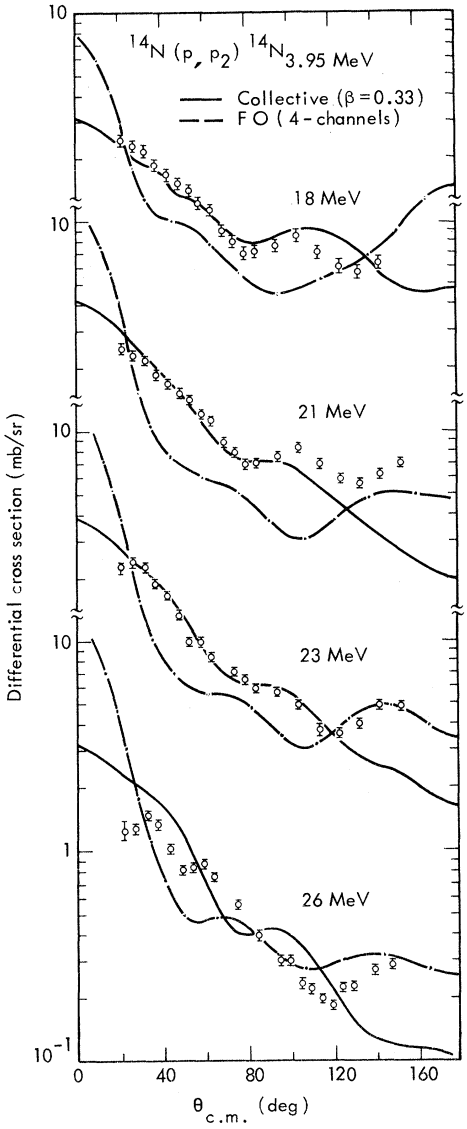

FIG. 12. Differential cross sections for the inelastic protons from the 3.95-MeV level measured (Ref. 10) at 18.0, 21.1, 23.0, and 26.0 MeV (Φ). The curves are a four-channel (1-2-3-4) microscopic calculation with Freed-Ostrander wave functions (—·—). The solid curve is a two-channel (1-4), macroscopic calculation with $\beta = 0.33$.

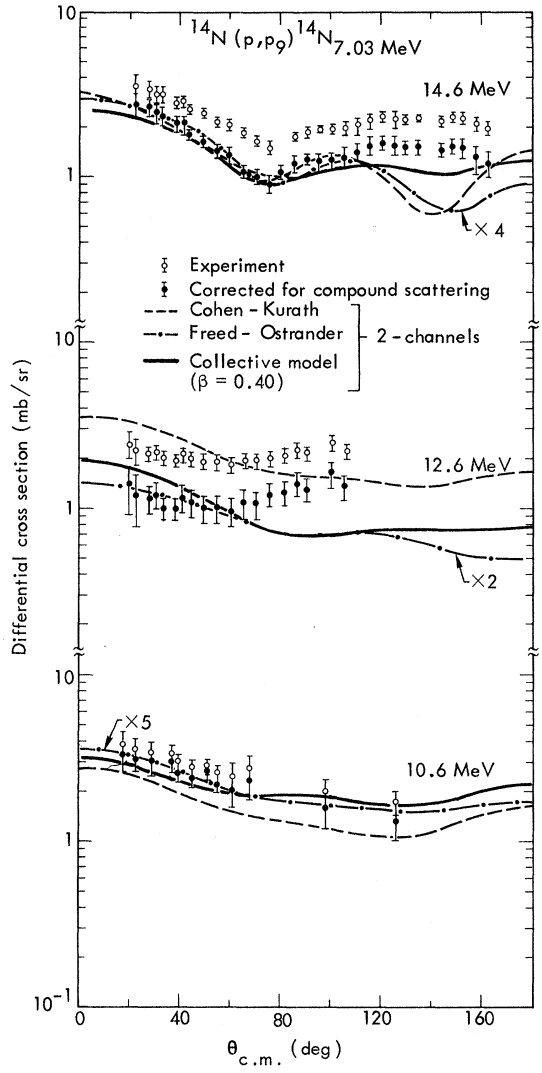

FIG. 13. Differential cross sections for the inelastic protons from the 7.03-MeV level measured at 10.6, 12.6, and 14.6 MeV (Φ). The filled circles are the measurements corrected for the calculated compound inelastic cross section to this level. The curves are a two-channel (1-5) microscopic calculation with Cohen-Kurath wave functions (---) and with Freed-Ostrander wave functions (—·—). The solid curve is a two-channel (1-5), macroscopic calculation with $\beta = 0.40$.

with exception of the 8.6-MeV data, the calculations reproduce reasonably well the experimental measurements corrected for the compound scattering given in Fig. 1. These compound corrections seem to overemphasize the dip close to 90°, but the subtraction method used here to correct the measurements is most sensitive to the magnitude of the correction at these angles where the difference between the measured and calculated compound cross sections is minimum. For the 8.6-MeV data, agreement is not expected since the measurements indicate a resonance structure. For the higher energies the best agreement with the measurements is obtained with Cohen-Kurath wave functions with the 2.31-MeV level coupled only to the gs. In Fig. 10 is shown a comparison between the DWBA calculation with Visscher-Ferrell wave function and the two-channel coupling using CK wave functions. The Freed-Ostrander wave functions give a reasonable agreement only at angles up to 80° except at 26 MeV, where it agrees reasonably well with the data at all angles. For the magnitude of the cross sections see Table IV.

The microscopic coupled-channel calculations for the 3.95-MeV level, given in Fig. 11 for the low energies, are those carried out with the simplest coupling: 1-4 (gs ^{14}N-3.95-MeV level), since the insensitivity of the calculations to the coupling was shown in Fig. 6. The differential cross section obtained with Cohen-Kurath wave functions and with the Freed-Ostrander wave functions are given. Although both calculations are rather poor, the Freed-Ostrander wave functions seem to give somewhat better agreement with the measurements when the compound-scattering corrections are carried out. Again, at 8.6 MeV, the angular distribution shows some resonance effects. For the higher energies[10] the best agreement in shape and magnitude is obtained with Freed-Ostrander wave functions shown in Fig. 12 for a four-channel coupling (levels 1, 2, 3, and 4 in Fig. 2). The magnitudes of the cross sections are given in Table V.

The calculations for the 7.03-MeV level are shown in Fig. 13 for Cohen-Kurath and Freed-Ostrander wave functions. Freed-Ostrander calculations have been multiplied by 5. For 14.6 MeV, both wave functions predict quite well the shape of the angular distributions corrected for compound scattering; for 12.6 and 10.6 MeV, the agreement is reasonable except for the normalization factor for the FO wave functions. No measurements for this level were reported for the higher energies.[10]

Macroscopic Model

In order to see if collective-model form factors, being complex and surface peaked, offer substantial advantages over the microscopic forms, a weak-coupling model of ^{14}N based on a ^{12}C core with two nucleons in the $p_{1/2}$ shell has been used. In this model the ground and 2.31 states of ^{14}N are generated by two $p_{1/2}$ nucleons coupled to the ^{12}C ground state, while the 3.95- and 7.03-MeV levels result from the coupling of these two nucleons to the 2^+ first excited state (4.43-MeV level) in ^{12}C, assumed to be a one-phonon vibrational state.

In this simple model the 3.95- and 7.03-MeV levels are not coupled to each other. Since no spin-dependent interaction is allowed, the transition to the 2.31 state cannot be included, nor can its coupling to the 3.95 state. Similarly, the $l=0$ spin-flip contribution was not included in the calculations of the gs → 3.95 transition.

The coupling matrix for the gs → 3.95 and gs → 7.03 transitions are vibrational form factors with strengths given by the relation

$$\beta_f = \beta_c \left(\frac{2S_f + 1}{(2J_c + 1)(2S_i + 1)} \right)^{1/2}, \tag{16}$$

where β_c and J_c are the deformation parameters, β_2, and the spin of the core, in this case the 4.43-MeV level in ^{12}C. Taking $\beta_2 = 0.60$ from Stelson and Grodzins,[41] the deformation parameters for the 3.95- and 7.03-MeV levels become 0.27 and 0.35, respectively. In the calculation, the values used are taken equal to 0.33 and 0.40, respectively.

The collective calculations obtained with the above assumptions are shown in Figs. 11, 12, and 13 by the solid line curves for the 3.95- and 7.03-MeV levels, respectively. For the 3.95 state at 14.6 MeV, the results reproduce the experimental values up to 70° rather well, and at 10.6 MeV, the over-all angular distribution. At higher energies the agreement is good in magnitude (Table V) and in shape, except at back angles. For the 7.03 state for the low incident proton energies, the agreement with the measurements is much better. At 14.6 MeV the collective model reproduces the measurements better than the microscopic calculation, since the large dip around 160° predicted by the microscopic model does not show in the macroscopic calculation.

CONCLUSION

From the results obtained in this paper, the following conclusions can be drawn: (1) Compound effects in the scattering of protons from ^{14}N are appreciable at proton energies less than 15 MeV. The direct calculations of the inelastic scattering at these energies agrees better with the measurements when they have been corrected for compound contributions. (2) A microscopic coupled-channel calculation differs from the DWBA only for the

scattering to levels with small cross sections. For strong transitions, the results are rather similar; the main effect of the coupling is to reduce the cross sections by as much as 20%. Similarly, the details of the couplings between the levels are important only for the weak transitions, the 2.31 level in our calculations, since the shape of the angular distributions is somewhat sensitive to the levels involved in the coupling. For the strong transitions, a two-channel coupling, the ground state and the final state are sufficient in the calculations. The near correctness of DWBA for the strong levels is substantiated by our results. (3) Pure p-shell wave functions such as those of Visscher-Ferrell and Cohen-Kurath give cross sections for the 2.31- and 7.03-MeV levels in fair agreement with the measurements, but they are unable to reproduce the shape of the cross sections for the 3.95-MeV level. Freed-Ostrander wave functions, where sd-shell configurations have also been included, do poorly for the 2.31-MeV cross sections as expected since they exclude the $p_{3/2}$ holes, which are required to explain the β decay of ^{14}C as was discussed earlier in Sec. C. They do better than the p-shell wave functions for the 3.95 level; the agreement with the measurements is marginal for energies below 15 MeV but greatly improved for the higher energies. The 7.03-level cross sections are very close in shape to those given by Cohen and Kurath, although the magnitude of the cross sections is lower by a factor of 5. (4) No normalization other than the exchange and the quadrupole corrections was needed for any of the cross sections calculated with Visscher-Ferrell and Cohen-Kurath wave functions. This indicates that the strength of the effective two-body force, given by the Kallio-Koltveit interaction, is rather good. (5) The strength of the tensor force $V_T = 4$ MeV also is a good choice as has been found by many others.[6, 10, 42] Trial calculations done with $V_T = 0$ or with somewhat larger values indicated that the value $V_T \approx 4$ gave the best results for the cross sections for the 2.31-MeV level. It was not necessary to introduce an energy dependence of the tensor force between 10 and 26 MeV for the strength of the potentials and ranges of the forces for the Kallio-Koltveit interaction (Table III) used in all these calculations. This suggests that the energy dependence observed by other authors[10] is the result of the different values of V_{11} and β_T used in their calculations.

ACKNOWLEDGMENTS

The authors would like to thank Dr. John D. Anderson, Dr. Virginia R. Brown, and Dr. Carl M. Shakin for stimulating discussions, Bert A. Pohl for making available to us the codes to calculate the spectroscopic factors from the different wave functions used in the calculations, Dr. Ted F. Harvey for helping with some of the computer problems encountered with the adaptation of the Oregon State coupled-channel code to the 7600 computer at Livermore, and Dr. Mitchell Gregory who helped in the initial stages of the measurements.

---

†Work performed under the auspices of the U. S. Atomic Energy Commission.

*Permanent address: Los Alamos Scientific Laboratory, P. O. Box 1663, Los Alamos, New Mexico 87544.

‡Permanent address: Oregon State University, Department of Physics, Corvallis, Oregon 97331.

[1]K. Matsuda, Y. Nagahara, Y. Oda, M. Takeda, N. Takano, T. Yamazaki, and C. Hu, J. Phys. Soc. Jap. 15, 760 (1960).

[2]R. E. Brown and D. G. Montague, Univ. of Washington Cyclotron Research Progress Report No. WAU-LIV-3A, 1963 (unpublished).

[3]P. F. Donovan, J. F. Mollennauer, and E. K. Warburton, Phys. Rev. 133, 113 (1964).

[4]S. Messelt, Phys. Norv. 4, 191 (1970).

[5]F. A. Schmittroth, Ph.D. thesis, Oregon State University, 1968 (unpublished).

[6]C. M. Crawley, S. M. Austin, W. Benenson, V. A. Madsen, F. A. Schmittroth, and M. J. Stomp, Phys. Lett. 32B, 92 (1970).

[7]C. W. Rogers, Oregon State University thesis, 1971 (unpublished).

[8]C. W. Rogers, P. Fessenden, and V. A. Madsen, Bull. Am. Phys. Soc. 16, 830 (1971).

[9]T. H. Curtis, H. F. Lutz, D. W. Heikkinen, and W. Bartolini, Nucl. Phys. A165, 19 (1971).

[10]H. F. Lutz, D. W. Heikkinen, and W. Bartolini, Nucl. Phys. A198, 257 (1972).

[11]M. J. Stomp, F. A. Schmittroth, and V. A. Madsen, the Oregon State coupled-channel code, contract No. AT (45-1)-2227.

[12]W. M. Visscher and R. A. Ferrell, Phys. Rev. 107, 781 (1957).

[13]S. Cohen and D. Kurath, Nucl. Phys. A101, 1 (1967).

[14]N. Freed and P. Ostrander, Nucl. Phys. A111, 63 (1968).

[15]A. Kallio and K. Kolltveit, Nucl. Phys. 53, 87 (1964).

[16]S. Cohen and D. Kurath, Nucl. Phys. 73, 1 (1965).

[17]F. S. Goulding, D. A. Landis, J. Cerny, and R. H. Pehl, IEEE Trans. Nucl. Sci. 11, 388 (1964).

[18]F. Bjorklund and S. Fernbach, Phys. Rev. 109, 1295 (1958).

[19]F. G. Perey, Phys. Rev. 131, 745 (1963).

[20]F. D. Becchetti, Jr., and G. W. Greenlees, Phys. Rev. 182, 1190 (1969).

[21]W. Hauser and H. Feshbach, Phys. Rev. 87, 366 (1952).

[22]A. C. Douglas and N. McDonald, Nucl. Phys. 13, 382 (1959).
[23]L. Wolfenstein, Phys. Rev. 82, 690 (1951).
[24]F. Ajzenberg-Selove and T. Lauritsen, Nucl. Phys. A114, 1 (1968).
[25]F. Ajzenberg-Selove, Nucl. Phys. A152, 1 (1970).
[26]S. M. Grimes, J. D. Anderson, A. K. Kerman, and C. Wong, Phys. Rev. C 5, 85 (1972).
[27]J. J. Schwartz, W. P. Alford, L. M. Blau, and D. Cline, Nucl. Phys. 88, 539 (1966).
[28]D. J. Baugh, G. J. B. Pyle, D. M. Rolph, and S. M. Scarrott, Nucl. Phys. A95, 115 (1967).
[29]R. H. Bassel, quoted by P. E. Hodgson, in *Proceedings of the International Congress on Nuclear Physics, Paris, 1964,* edited by P. Gugenberger (Centre National de la Recherche Scientifique, Paris, France, 1964), Vol. 1, p. 257.
[30]R. W. Bauer, J. D. Anderson, H. F. Lutz, C. Wong, J. W. McClure, and B. A. Pohl, Nucl. Phys. A93, 673 (1967).
[31]J. L. Alty, L. L. Green, R. Huby, G. D. Jones, J. R. Mines, and J. F. Sharpey-Schafer, Phys. Lett. 20, 664 (1966).
[32]G. R. Satchler, Phys. Lett. 7, 55 (1963).
[33]P. A. Moldauer, Phys. Rev. 135B, 642 (1964).
[34]J. P. Schiffer, G. C. Morrison, R. H. Siemssen, and B. Zeidman, Phys. Rev. 164, 1274 (1967).
[35]V. A. Madsen, Nucl. Phys. A80, 177 (1966).
[36]F. Petrovich, H. McManus, V. A. Madsen, and J. Atkinson, Phys. Rev. Lett. 22, 895 (1969).
[37]H. J. Rose, O. Häusser, and E. K. Warburton, Rev. Mod. Phys. 40, 591 (1968).
[38]J. D. Anderson, C. Wong, and V. A. Madsen, Lawrence Livermore Report No. UCRL-50197 (unpublished).
[39]V. A. Madsen, *Nuclear Spectroscopy and Reactions,* edited by J. Cerny, III (Academic, New York, to be published).
[40]J. Atkinson and V. A. Madsen, Phys. Rev. Lett. 21, 295 (1968).
[41]P. H. Stelson and L. Grodzins, Nucl. Data A25, 21 (1965).
[42]C. Wong, J. D. Anderson, V. A. Madsen, F. A. Schmittroth, and M. J. Stomp, Phys. Rev. C 3, 1904 (1971).